Energy Conversion and Management 84 (2014) 244–252

Contents lists available at ScienceDirect

Energy Conversion and Management

journal homepage: www.elsevier.com/locate/enconman

Thermoelectric topping cycles for power plants to eliminate cooling water consumption

Kazuaki Yazawa [a,*], Menglong Hao [b], Bin Wu [c], Armin K. Silaen [c], Chenn Qian Zhou [c], Timothy S. Fisher [a,b], Ali Shakouri [a]

[a] Birck Nanotechnology Center, Purdue University, West Lafayette, Indiana 47907-2057, United States
[b] School of Mechanical Engineering, Purdue University, United States
[c] Center for Innovation through Visualization and Simulation, Purdue University Calumet, United States

ARTICLE INFO

Article history:
Received 15 January 2014
Accepted 9 April 2014
Available online 4 May 2014

Keywords:
Thermoelectric
Topping cycle
Rankine cycle
Power generator
Boiler
Steam temperature

ABSTRACT

This work shows that thermoelectric (TE) topping generators can add 4–6% to the overall system efficiency for advanced supercritical steam turbines (Rankine cycle) that nominally generate power with 40–42% efficiency. The analysis then considers how this incremental topping energy can replace cooling water flow with air-cooled condensers (ACC) while maintaining current power output and plant efficiency levels with commensurate economic benefit ($/kW h). The simulated TE modules are located inside a coal-fired boiler wall constructed of wet steam tubes. The topping TE generator employs non-toxic and readily available materials with a realistic figure-of-merit range (ZT = 0.5–1.0). Detailed heat transfer and thermal analyses are included for this high-temperature TE application (e.g., 800 K for the cold side reservoir). With the tube surface enhanced by fins, the TE elements are designed to perform optimally through a distributed configuration along the wall-embedded steam tubes that are more than 20 m high. The distribution of the gas temperature in the furnace along the wall height is predicted by thermo-fluid dynamic analysis. This foundational design and analysis study produces overall realistic efficiency predictions in accordance with temperature–entropy analysis for superheated Rankine cycles. Lastly, the approach also allows for the addition of waste heat recovery from the flue gas. The analysis shows that the power output from the topping TE generator is significantly larger, compared to that from the waste heat recovery, due to the larger available temperature difference.

1. Introduction

Improved energy efficiency of power production is still important for most common coal-fired power plants, which provide 50.4% of electricity supply in the U.S. [1] while the penetration of renewable energy sources remains hindered by capital cost, intermittency, and seasonal swings [2,3]. Some large solar concentrated power plants using Rankine cycles operate primarily in desert areas [4]. Energy efficiency is not only important for economic reasons, but it is also critical for conserving natural resources [5]. We investigate the performance and economic impact of adding thermoelectric (TE) topping generators to provide additional power output from current-technology coal-fired boiler furnaces within an advanced supercritical steam turbine (Rankine cycle).

Fig. 1 shows results from a prior analysis for a combined cycle [6], which indicates an optimum steam temperature for maximizing total output power. This additional power output can cover the deficit in power output by higher temperature condensation utilizing an air-cooled condenser [7]. There is another way to enhance the total power output by utilizing a waste heat recovery cycle either by thermoelectric or other energy conversion principle. The waste heat recovery can coexist with the topping cycle without mutual interference. Waste heat recovery TE generators for automotive exhaust applications [8,9] require some exotic materials, about figures-of-merit (ZT) of 1.5–2, to realize performance improvements of practical utility. In contrast, topping TE generators for higher temperature range could consist of non-exotic and readily available materials with thermoelectric with ZT of unity or less, due to the larger available temperature difference. Furthermore, the energy not converted by TE generators is used for the steam turbine. However, the associated high temperatures (e.g., >800 K for the cold side) have, so far, precluded commercialization of TE topping cycles. Here we investigate thermoelectric materials and a thermal design based on the dimensions and conditions of a real boiler existing in a power plant.

* Corresponding author.
E-mail address: kyazawa@purdue.edu (K. Yazawa).

http://dx.doi.org/10.1016/j.enconman.2014.04.031
0196-8904/

Nomenclature

A	area (m^2)
d	thickness of thermoelectric leg (m)
D	diameter (m)
F	fill factor (fractional area coverage of thermoelectric element) (–)
m	load resistance ratio (ohm/ohm)
Q	heat (W)
s	entropy (J/kg K)
T	temperature (K)
W	electric power [W]
x	height along the boiler chamber (m)
Z	figure of merit of thermoelectric (1/K)

Greek symbols

η	efficiency (–)
ψ	thermal resistance (K/W)

Subscripts

F	flue gas cycle
g	steam temperature
in	input
s	source (flame) temperature
ST	steam turbine
T	topping cycle
TE	thermoelectric

Abbreviations

ACC	air cooled condenser
CTE	coefficient of thermal expansion
FGD	flue gas discharge
JPL	Jet Propulsion Laboratories
NASA	National Aeronautics and Space Administration
ODS	oxide dispersion strengthened
RTG	radioactive thermoelectric generator
T-s	temperature-entropy
TE	thermoelectric
TP	topping cycle
WHR	waste heat recovery

Fig. 2 illustrates the system schematic of a current state-of-the-art 520 MW class power plant unit, including the cooling portion enclosed in a dashed line. This subsystem is of particular importance in minimizing water resource usage. To enable a realistic and practical evaluation, we analyze the fluid-dynamic behavior of the gas in the furnace and solve the conjugate heat transport by thermo-fluid dynamic modeling. With surface area enhancement, the TE modules are designed between the wall of the boiler and the water tubes. The TE elements are optimized locally for the simulated gas temperature profile, which is graded along the wall height of over 20 m. These basic designs and analysis enable the prediction of a realistic overall efficiency in accordance with temperature-entropy (T-s) diagram analysis for a complete superheated Rankine cycle.

2. Boiler thermo-fluid analysis

Power plants burn fossil fuel and turn water into steam, which is then used to move turbines and generate electricity. Typically, water is circulated inside tubes around the wall of the furnace (boiler). In a subcritical boiler, the water/steam mixture leaving the tube risers is separated into water and steam. The water returns to an evaporator inlet, and the steam flows into a superheater. The superheater raises the steam temperature to avoid the formation of water droplets when the temperature drops due to expansion in the steam turbine. In a supercritical boiler, water enters the boiler above the critical pressure (22 MPa) and is heated to a temperature above the critical temperature (647 K). The water does not boil as it is heated, but rather decreases in density until it becomes vapor. The thermodynamic efficiency of a power plant using supercritical steam is typically higher (40–42%) than that of a similar subcritical plant (36–38%).

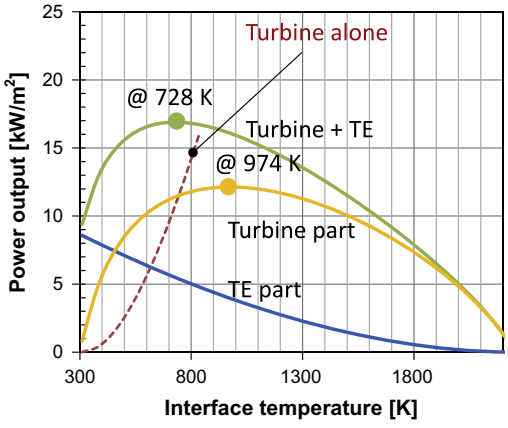

Fig. 1. Power output as a function of the interface temperature between a TE module (with ZT ~ 1) and the steam temperature in Rankine cycle (Ref. [4]). The green curve shows the system total power output while the red dashed curve shows the Rankine cycle (steam turbine) which is limited by the steam temperature.

Power plant modeling can incorporate issues ranging from flow optimization to simulation of different operating conditions using state-of-the-art, high-fidelity thermodynamic models in addition to new water conservation and water treatment technologies [5]. One such example is a 1943 MW coal-fired power plant that includes two subcritical boilers and two supercritical boilers (one of the latter is shown in Fig. 3). The facility uses pulverized coal in ten burners. The combustion products heat the burner walls, and the heat energy is transferred primarily by radiation. When the flue gas leaves the burners, the heat energy in the gas is transferred to the tubes located along the furnace wall by convection. The gas temperature reaches 1700 K, but the steam temperature leaving the boiler is only 640 K.

A numerical study has been performed to calculate the impact of thermoelectric modules on the walls of the boilers and to estimate the total output power [10]. Fig. 4 below shows the temperature distribution near the boiler wall obtained from a computational fluid dynamics model. The 5.1 million cell meshes were generated based on the 3D model for calculating flow regime and temperature distribution. The conjugate problem is solved with popular k-ε turbulent model. Based on the gas temperature distribution, four different locations with different gas temperatures (1680 K, 1500 K, 1300 K, and 1150 K) inside the boiler were used for the thermoelectric power generation analysis. At each location the thermoelectric leg thickness was optimized to obtain the maximum power output. The results show that the thermoelectric module at those four locations can increase the local work output per unit area by 7.1%, 7.0%, 5.6% and 4.4%, respectively. Increased thermal resistance by the TE generator requires the

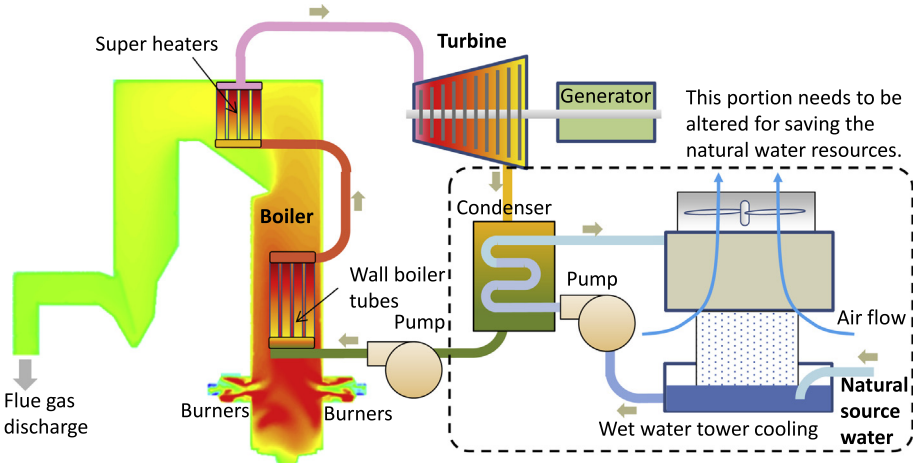

Fig. 2. Current state-of-the-art supercritical steam turbine with 520 MW_e power output.

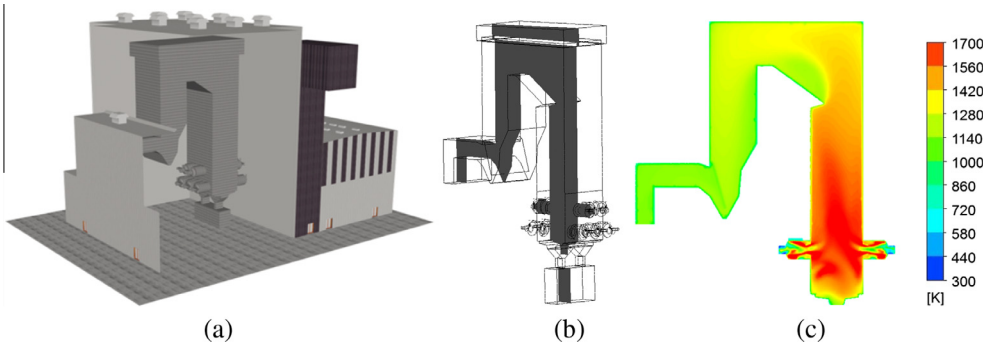

Fig. 3. (a) 3D cutaway of a coal-fired powerplant with one of its supercritical boilers, (b) 3D geometry of the boiler, and (c) calculated gas temperature distribution inside the supercritical boiler [10].

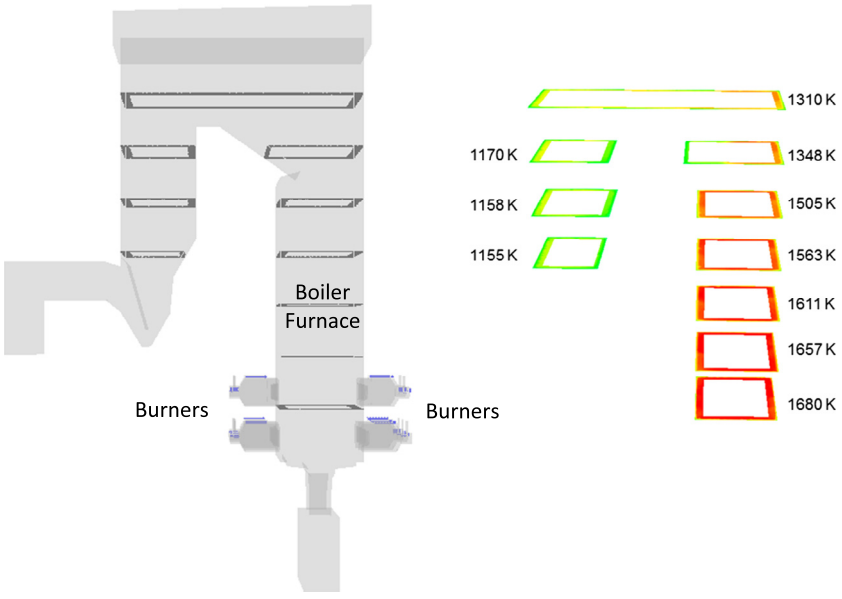

Fig. 4. Gas temperature near the boiler wall.

addition of fins to the hot side of the TE module to conserve the amount of heat flux. Alternatively, one can, modify the cross sectional area of the boiler and its surface-to-volume ratio. The geometry of the boiler, fin structures, and TE module thermal impedance should also be optimized for maximum performance.

3. Thermoelectric topping cycle optimization

The alternate system diagram proposed in this analysis is shown in Fig. 5. The water-cooled condenser units (heat exchangers) are replaced by dry cooling air cooled condenser (ACC) units.

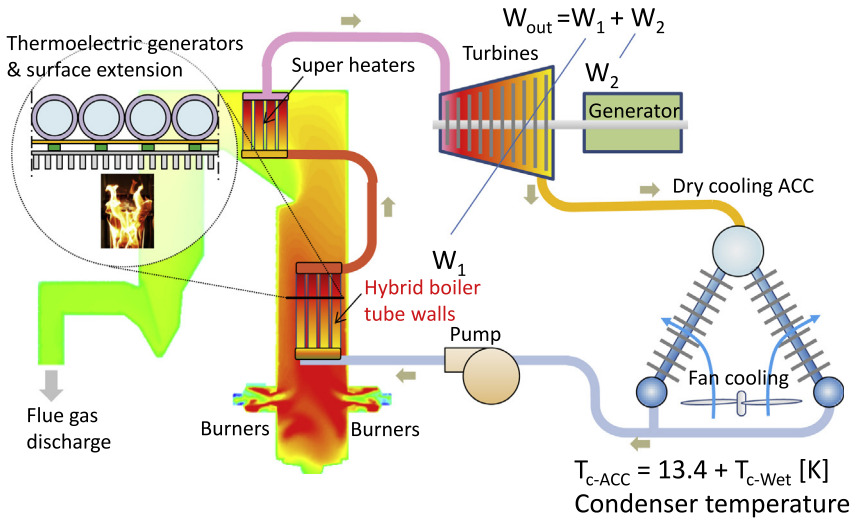

Fig. 5. Thermoelectric implementation concept diagram. The values are based on current existing power plant and optimum design of TE modules with ZT = 0.6. The thermoelectric generators are located facing interim boiler surrounded by the steam tubes.

Due to the higher condensation temperature in the ACC, the temperature of the condensed steam increases by 12–15 K [5]. According to Ref. [11], a 13.4 K temperature increase in the condensed steam temperature reduces thermodynamic efficiency by 5%. This change is shown in temperature–entropy (T-s) diagram shown in Fig. 6 with dotted line in the bottom of the cycle. Note that this particular Rankine cycle is using the super heater and the steam power is used for turbine generator in supercritical phase. The above efficiency degradation is compensated by adding high-temperature TE generator modules placed between the hot gas and the boiler wall steam tubes. This additional power generated by TE on top of the operating temperature range of a Rankine cycle generator helps in introducing ACC for saving natural water. Pump efficiency as a function of water temperature is not considered in this analysis. The change in viscosity of water is reduced by 20% for the 13.4 °C temperature increase. Hence, the pressure loss may be smaller. We assume that the slight increase in water temperature would not have a negative impact on the system efficiency. In the following we will describe the optimum design of the TE generator.

We surveyed the literature for thermoelectric materials that can meet the operating temperature range. For large scale implementation, it is also important to consider non-toxic and abundant materials. Historically, radioisotope thermoelectric generators (RTGs)

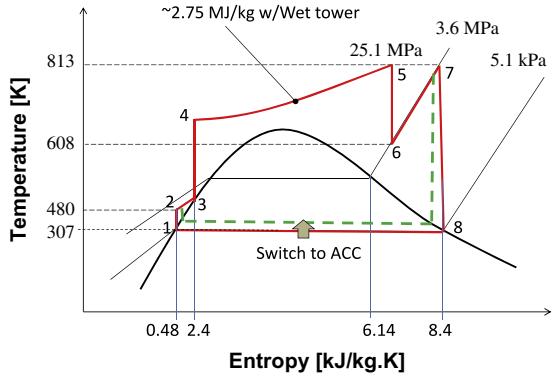

Fig. 6. Temperature (T) – entropy (s) diagram of a real power plant. This particular advanced Rankine cycle system includes two-stage turbines (2-3-4 with the superheater and 5-6-7 with the economizer) to broaden both the temperature and the entropy range.

have been successfully used to power a number of NASA space missions. The RTGs operate between 1273 K (hot side) and 566 K (cold side). RTGs typically use silicon germanium (SiGe) alloys as TE elements. The system-level conversion efficiency for state-of-the-art RTGs is about 6% with lifetimes in excess of 30 years [12]. We base our proof-of-concept demonstration on well characterized SiGe material [13,14]. The SiGe used for spacecraft applications can be improved, and its figure-of-merit (ZT) has been increased to ZT = 1 via nanostructuring, which decreases thermal conductivity without substantially changing the electrical properties [15]. Germanium however, is a less abundant material and unfortunately not practical for large-scale deployment in power plant applications. The use of SiGe will also slightly limit the highest operating temperature at the hot side of the TE leg. State-of-the-art p-type $Yb_{14}MnSb_{11}$ and n-type $La_{3-x}Te_4$ have demonstrated maximum ZTs in the range of 1.2–1.5 at 1300 K and are being actively pursued by NASA JPL for space applications but these are not abundant either. Trading-off the performance, nanostructured silicon materials could be considered as they have reasonable ZTs (0.3–0.4) at high temperatures. Given the variability in ZT levels as well as practical material considerations, we use ZT as an adjustable parameter within the practical range described above.

We subsequently investigate the design of the thermoelectric module and the potential parasitic losses. Based on preliminary calculations presented in Ref. [16], the optimum TE leg thickness for the particular boiler described in Section 2, should be approximately 1.3 mm considering currently available SiGe with 10% fractional area coverage of TE legs inside the module. This will require a metal/semiconductor contact resistivity in the range of 10^{-5} ohm-cm^2, which has been achieved [17]. Also, thermal parasitic losses need to be considered through the non thermoelement area via radiation heat transfer and gap material (usually air) heat conduction. Based on Ref. [17], these parasitic losses are less than 10% of the heat conduction through the thermoelements with 10% fractional area coverage. If it is needed, a partial vacuum ranging 5 millibars or a coating with reduced emissivity by 0.3 may reduce the loss contribution less than 2% for each. Next, we analyze the overall system efficiency and cost.

3.1. Reduction of mechanical stress in the TE module

In addition to the functional (thermal) performance, the mechanical robustness of the proposed TE system must be

addressed. Effective predictive modeling includes analytical (mathematical) and numerical, usually finite-element-analysis (FEA), simulations. Thermal loading caused by the different and variable TE's hot and cold side temperatures, is a major contributor to the possible mechanical failures in the system. The induced stresses are due to the temperature gradients in the module structure, as well as to the different coefficients of thermal expansion (CTE) of the dissimilar materials in the TE subsystem. The major thermal stress categories include normal stresses acting in the cross-sections of the plates and shearing and peeling stresses acting at the material interfaces. Based on earlier work carried out for assemblies with inhomogeneous bonding layers, it is the maximum interfacial shearing stress that must be considered as the most crucial thermal stress to be evaluated and minimized for the highest possible TE robustness [19,20]. As described in these papers, it is possible to achieve large temperature gradients in topping cycle applications with the use of modules of low fractional area coverage of TE elements (F = 10%, Table 2). The thickness of the hot and cold plates and metal interconnects is an important design variable. The stress in the whole TE module integrated with steam tubes can be optimized using analytical models and FEA.

4. Heat exchanger enhancement at high temperatures

Fig. 7 shows a concept schematic of placing TE generators as a topping cycle between the hot gas and the bundled steam tubes on the interior surface of the boiler wall. To compensate the increasing thermal resistance when the TE generator is added, fin surface is considered to enhance the heat transfer coefficient so that total thermal resistance from the hot gas to the steam in the boiler tube is maintained constant.

Conventional TE systems consist of many integrated elements, including thermal, mechanical, and electrical components and sub-systems. The overall performance of a TE system is determined by the thermal profile in, as well as the figure-of-merit (ZT) of the TE materials. For both technical and non-technical endeavors, a system is often only as strong as its weakest link, and interfaces commonly play this role. Integration of heterogeneous materials that require robust and precise electrical and thermal interconnections in such a harsh thermal–chemical–mechanical environment poses a major challenge with this approach.

The hot-side (i.e., gas-side) heat exchanger design is expected to be particularly challenging. A one-dimensional model indicates that the hot junction temperature will be greater than 1000 °C when thermoelectric modules are producing maximum output. As compared to traditional boiler water tube configurations, a customized fin design is required to minimize thermal resistance through combined radiative and convective pathways. Radiation heat transfer enhancement, such as durable surface coatings with high emissivity values, is needed to take full advantage of the high combustion temperatures. An associated challenge regarding the heat exchanger involves material selection. At the desired temperature (>1000 °C), traditional metallic materials, mainly stainless steel and nickel alloys, can no longer be used. Experience in the nuclear industry, where similar heat exchangers are also required, suggests two main material classes: oxide dispersion strengthened (ODS) alloys and ceramics [21]. ODSs are composite materials with metal–matrix and oxide reinforcement (often Y_2O_3). The high-temperature strength of this material class is significantly better than that of metallic counterparts due to the pinning of grain boundaries that impede creep [22]. We also note that this class of materials and their oxide coatings inherently possess high radiative emissivity ($\varepsilon > 0.9$) [23].

Due to the limited flexibility of designing heat sinks in the boiler, Thermal interfaces play a major role for maximizing the power output. Thermal interface materials must result in low thermal contact resistance, to optimize the overall thermal profile and provide high energy-conversion performance. The greatest challenge for the present application relates to the large temperature differences produced by the high-quality heat source. This application has two major issues: (1) instability of traditional thermal interface materials; and (2) very large thermal strains that compromise the integrity of the bonded interfaces. A possible solution involves a variant of brazing that incorporates a fibrous matrix to enable the ability to take up thermal strains through both deformation and mechanical bearing behavior. The challenge in the present work is extreme, as solutions are needed for temperatures as high as 1300 °C. Zorc and Kosec [24] developed a hybrid brazing approach and reported a dramatic improvement in thermo-mechanical stability and joint toughness through the use of wire reinforcement. In essence, as in woven composites, the composite structure arrests crack propagation to enhance durability.

Carbon nanotube (CNT) arrays have been used as a fibrous component for conventional thermal interfaces [25–27], but the thermal stability of graphitic materials is inadequate for the present application. Other carbon material could be applied in a matrix form; for example, Cao and Chung [28] observed up to 300% improvement in shear strength at room temperature with the addition of carbon fibers to a silver–copper braze in a ceramic–metal joint.

Thermal interfaces for moderate-to-high temperature applications must also be able to withstand large and frequent temperature fluctuations over many years of operation. Further, thermal interface metrology techniques are not well established for the anticipated high temperature range. Most existing thermal interface studies target applications in electronic cooling and are therefore, limited to the low-to-medium temperatures [29,30]. In the limited number of studies that report thermal interface resistance at high temperatures [31,32], the laser flash method has often been selected. Its validity however, for this type of measurement, as Absi et al. [33] note, is questionable due, primarily, to its assumption of a homogeneous material. Some contemporary thermal interface test methods, mainly including the 3ω [34], thermoreflectance [35], and steady-state reference bar [36,37] methods, have the potential to be extended to higher temperatures as long as

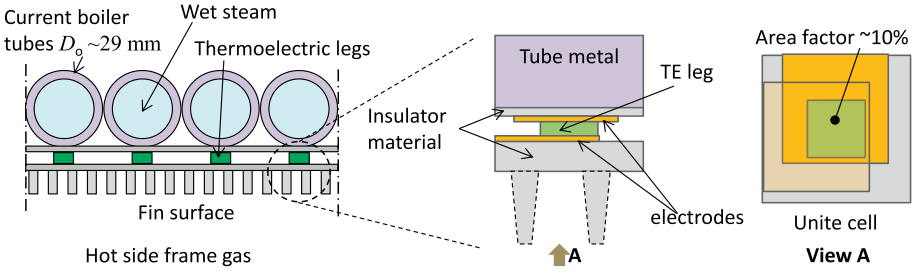

Fig. 7. Conceptual schematic of the simplified TE module with 10% fractional coverage integrated on top of steam tubes inside boiler walls.

radiation heat loss can be carefully calibrated or effectively suppressed. Jensen et al. [38] modified the steady-state reference bar method to measure thermal conductivity in an extended temperature range and concluded that uncertainty is within 6% for 100–800 °C with samples having thermal conductivity of 10–70 W/mK.

5. Flue gas energy recovery

Flue gas discharge (FGD) at temperatures above ambient also presents an opportunity for thermoelectric generators to harvest wasted heat energy. For a plant without a FGD scrubber, discharged flue gas is typically at 180 °C for either ordinary or supercritical boilers [39]. This temperature, when combined with cold feed water from an ACC or ambient air as a heat sink, provides a reasonably large temperature difference to drive thermoelectric generators assuming all waste heat in the flue gas is utilized by thermoelectric modules made from a material with a ZT ~ 1, e.g. the bismuth-telluride (Bi_2Te_3) or led-telluride (PbTe). Higher ZT materials compared to that of the topping cycle TE material are also readily available for this temperature range. It should be noted that another 0.5% of energy from the fuel combustion could be converted to electricity with the design maximizing power output from the thermoelectric generator based on above heat source temperature (180 °C). Another advantage of harvesting this waste heat with thermoelectric generators is that moisture in the flue gas would condense as its temperature decreases. For the case where the plant is water-cooled, this extra water can be utilized with the potential to provide 10–20% cooling tower makeup water. This is calculated based on baseline Case 11 described in [39], assuming the flue gas can be cooled to temperatures very close to that of the ambient. Introducing the heat exchangers may require additional power to maintain the gas flow. The hot gas flow through the fins is especially important for power generation. Fortunately, the pump power required for the flue gas is orders of magnitude lower compared to the generating power based on [40], for heat fluxes in the a range of 10^{+4} W/m^2, which we estimate for this case.

Due to the relatively small temperature difference compared to that of a TE topping cycle, a lower conversion efficiency and system power density is anticipated for flue gas wasted heat recovery. Further, the low thermal power density would require thicker thermoelectric elements and therefore associated capital cost per power converted is significantly higher than that of the topping cycle.

6. System efficiency analysis

6.1. System efficiency analysis

The following analytic modeling based on the design of thermoelectrics for the maximizing the system efficiency is plugged in a temperature–entropy (T-s) model to estimate the power plant efficiency without consuming natural water resources as shown in Fig. 5. The system efficiency is determined by total power output per heat input, the total power output counts the power from thermoelectric modules in addition to the steam turbine. The heat input to the steam turbine is reduced by the efficiency of topping TE according to the following analysis.

$$\eta = \frac{W_{\text{TE-T}} + W_{\text{ST}} + W_{\text{TE-F}}}{Q_{\text{in}}} = \eta_{\text{TE-T}} + (1-\eta_{\text{TE-T}})\eta_{\text{ST}} + (1-\eta_{\text{TE-T}})(1-\eta_{\text{ST}})\eta_{\text{TE-F}} \quad (1)$$

where the subscripts TE-T indicates topping thermoelectrics, TE-F indicates FGD thermoelectrics, and ST indicates the steam turbine, respectively. An important contribution of the topping cycle could to reduce the heat input to the boiler while the FGD cycle does not. This heat reduction can also help to reduce the cooling load and the additional power covers the power output reduction resulting from the condenser replacement to ACC for saving the water.

Local maximum power output $W_{TE\text{-}T}$ for a local gas temperature T_s is found by the following expression according to Ref. [17], knowing that the sum of the thermal resistances is $\Sigma\psi$, which includes contributions from the hot gas side and the contact to the boiler tube and heat conduction through the boiler tube wall. The local maximum power output with local heat source temperature T_s requires optimizing the thickness of TE element locally. The coefficient ¼ in the equation is valid if the thermal resistances of hot and cold sides are similar. This coefficient is insensitive to the difference between thermal resistances of the hot side and the cold side. In an existing 520 MW supercritical Rankine cycle system, the heat transfer coefficient at the hot side is 246 [W/m^2 K] and the one at the cold side is 722 [W/m^2 K], respectively, see Ref. [10]. To add the TE generator, heat transfer for the hot side must be enhanced by a factor of three. The difference in maximum power output is only 0.2% compared to the case where both thermal resistances are exactly the same. Even without afin and using the original heat transfer coefficient (e.g. threefold increase in thermal resistance), the resultant change in output power is only 8%. The expression for TE power then becomes,

$$W^*_{\text{TE-T}} \cong \frac{Z}{4(1+m)^2\sum\psi}(T_s - T_g)^2 \quad (2)$$

where T_g, is the steam temperature in the boiler tube and m is the ratio of electrical load resistances to the internal resistance of the TE element. The optimum TE leg thickness d_{opt} for the maximum power output is found as,

$$d_{opt} = m\beta FA\sum\psi \quad (3)$$

where m is the load resistance ratio, β is thermal conductivity of TE material, F is fractional area coverage of TE leg ($F \sim 10\%$ in practice [18]), A is the area assigned for one TE leg. Note that we can design the array of legs so that the smaller A provides a smaller thickness d.

The overall power from the topping thermoelectric is found by taking an integral across the entire temperature range along the boiler height from x_1 to x_2. The overall power output from the topping thermoelectric module array becomes,

$$W_{TE-T} = \frac{Z}{4(1+m)^2\sum\psi}\left(\int_{x_1}^{x_2}(T_s(x)-T_g)^2dx\right)\Big/\left(x_2-x_1\right) \quad (4)$$

Also the flue gas thermoelectric power produces the following work, if applicable,

$$W_{TE-F} = \frac{Z}{4(1+m)^2\sum\psi}(T_F - T_w)^2 \quad (5)$$

where T_w is the water temperature returning from the ACC units and T_F is typically 180 °C.

Reduction of the heat input to the steam turbine by adding the topping generator as shown in Eq. (1) could work for reducing the required cooling capacity for condensers. This power output margin provides an allowance for the refrigerant temperature returning to the compressor from the condenser to be higher and also provides a possibility to switch to the ACC units from the tower cooling units. The condenser modification changes the T-s cycle profile as indicated previously in Fig. 6. With a new temperature profile, T' derived from the alternate condenser, ACC, the power output from the turbine is found by taking the integral of the closed area in the T-s diagram in Fig. 6 as,

$$W'_{\text{ST}} = \oint T'ds \quad (6)$$

Table 1
Thermoelectric material properties.

Material	Thermal conductivity, W/m K	Electrical conductivity, 1/Ohm m	Seebeck coefficient, μV/K	Density, kg/m^3
SiGe (TE-TP)	3.5	2.3e + 4	300	3827
PbTe (TE-WHR)	2.5	9.0e + 4	270	8160

Table 2
Cooling cost estimates by method based on a "500 MW_e class" power plant.

System	Power output	Cooling equipment cost	Source
Current w/wet tower	520 MW_e	US$12.5 M (Steam condenser $2.5 M + tower $10 M)	Ref. [11], Table 3–3
Hybrid w/ACC	520 MW_e	US$93 M (TE $3 M + ACC $90 M)	Ref. [11], Tables 3–6 and Table 2

Note: The hybrid system is adapted to the condenser temperature induced by the ACC.

To maintain the total power output (without considering waste heat recovery from FGD), this alternate steam turbine power output must satisfy $(1-\eta_{TE-T})\eta_{ST}Q_{in}$ at least. The temperature change by converting the condenser with an ACC is 13.4 °C, based on Ref. [11], and it may cause 4–5% power output reduction from the steam turbine with a cooling tower condenser. This power degradation is covered by adding the topping TE generators.

For an example performance calculation, we used the ZT values of currently available materials, but they are not necessarily the material for large scale deployment. A nanostructured SiGe, [41] ($ZT \sim 0.7$) is considered for the topping cycle TE and a lead-telluride (PbTe), [42] ($ZT \sim 1.0$) is considered for the waste heat recovery from the FGD. Material properties of the thermoelectric materials are listed in Table 1. For an accurate analysis, the temperature dependencies of the material properties cannot be neglected for the relatively large temperature differences in this study. Here we focus on an "average" ZT over the whole temperature range in order to understand the basic trends and how the topping cycle can impact the overall performance. Hence, the following material properties are picked from typical values in the reference and considered at the mean temperature.

The topping cycle TE generator system is designed to maintain the baseline heat flux through the boiler wall so that the Rankine cycle is not changed. As shown in Fig. 6, the heat transfer coefficient for the hot side is extended by factor of three. Hence heat transfer coefficients are 738 W/m^2 K for hot side and 722 W/m^2 K for the cold side. For the FGD waste heat recovery, the heat transfer coefficient is assumed to be both 246 W/m^2 K, which is the same as the cold side for the topping cycle. To match the overall heat flow, areas of the additional generators are found to be 8541 m^2 for the topping generator and 82,745 m^2 for the waste heat recovery generators, respectively. In the boiler, hot gas temperature changes depending on the height as shown in Fig. 4. The gas temperature in applicable section for topping TE is ranging from 1500 K up to 1680 K. Fig. 8 shows the conversion efficiency and the power output per unit area as functions of gas temperature. The power output is larger at the higher gas temperature with a parabolic dependence as expected from Eq. (2). The TE element thickness d is always optimized to generate the maximum power at any location. Fill factor is fixed to 10%. Due to the hot side temperature is changing along the height location in boiler, ZT value is slightly decreasing by 7% as increasing height or decreasing gas temperature without considering the temperature dependence of the material properties.

6.2. Economic analysis

A thermoelectric module with a smaller fill factor, F, (fractional area coverage of the thermoelectric element to the substrate) can result in a significantly lower initial cost to build. Without regard to changing the fill factor, the internal thermal resistance of the TE element is designed to match the external one. Hence, the smaller fill factor, in a range not less than 10%, essentially reduces the thickness linearly. The material cost is proportional to F^2 and will be negligible even considering the use of a relatively expensive thermoelectric material. The cost of the thermoelectric material, SiGe, for the topping cycle is dominated by the market price of Germanium ~$2000 per kilogram and the cost of PbTe $500 per kilogram is assumed based on industrial input for a large-scale mass production.

For an example, to replace the current cooling tower condensers with ACC units, the initial cost increases by $79.5 M for a 500 MW_e class power plant (see Table 2). Based on $0.05 per kW h for the baseline electricity price and 30 years of operation, this initial cost is only ~1% of the overall system investment.

Since fresh water is not always available locally, the cost of local cooling water falls between $0.0 and $6.8 M per year for a 500 MW_e class power plant based on the commercial pricing of water, (approximately $2 per 1000 gallons) and based on a 6000 gallons per minute of flow rate [43]. Allowing the use of an ACC, the total power output remains the same for the same heat input (fuel input). Therefore, there will be no improvement or no additional fuel to burn. This approach does not add any penalty for the global warming impact or increase CO_2 emission as an environmental impact.

The cost details of TE generators are shown in Tables 2 and 3 followed by an overall performance and cost comparison shown in Table 4. The current Rankine cycle system is compared with the cases that are; (1) with topping TE generator (TE_TP), (2) with waste heat recovery TE generator (TE_WHR), and (3) with both TE generators (TE_TP&WHR). If the TE generator for waste heat

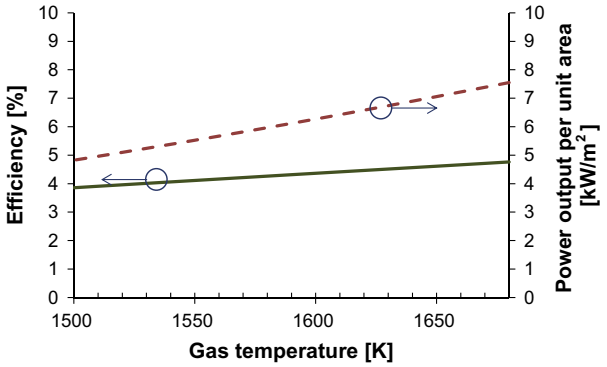

Fig. 8. Efficiency and the power output per unit area as functions of local gas temperature along the height of boiler. Power output shows in parabolic relation to the gas temperature. ZT value is 0.7 at mean temperature. The TE thickness is always optimized by location.

Table 3
Details of TE topping generator with 31.0 MW_e output.

Elements	Material	Material price	Dimensions	Mass
Thermoelectric (TE)	SiGe	US$2000/kg	F = 10%, t = 1.3 mm	4.3 ton
High temperature heat fins, substrate for TE elements	Mo	US$20/kg	Area 8541 m^2, t = 0.2 mm & fins	35.1 ton
Surface coating	Al_2O_3/TiO_2	US$2/kg	t = 20 μm	675 kg

Table 4
Details of the TE waste heat recovery with 22.4 MW_e output.

Elements	Material	Material price	Dimensions	Mass
Thermoelectric (TE)	PbTe	US$500/kg	F = 10%, t = 2.9 mm	197 ton
High temperature heat fins, substrate for TE elements	Al_2O_3	US$2/kg	Area 82,745 m^2, t = 0.2 mm	131 ton

Note: F stands for fractional area ratio and t stands for thickness.

Table 5
Overall comparison.

	Total power output				Additional initial cost		
	Tower		ACC		TE mass	Mat. Cost	Cost/power
	MW	Increment	MW	Increment (%)	ton	$ million	$/W
Current	**520.0**	–	494.0	−5.0	–	–	–
TE_TP	551.0	6.0%	526.1	1.2	4.3	9.26	0.299
TE_WHR	542.4	4.3%	515.3	−0.9	197.1	98.84	4.408
TE_TP + WHR	572.4	10.1%	546.5	5.1	201.4	108.10	2.062

The bold value shows the baseline.
Note: Subscripts TP stands for topping cycle and WHR stands for waste heat recovery from the FGD. 'Mat.' stands for material. Tower stands for water cooling tower for the condenser and ACC stands for air cooled condenser. The values are based on the heat input equivalent to 520 W_e of power output from the base line, which is the current superheated steam turbine generator. The TE-WHR in this case is used for all of the available waste heat. In practice this may be limited by the area or the cost.

recovery uses 100% of available heat in FGD, it occupies almost 10 times of the area compared to the topping TE in boiler section. The overall comparison shown in the Table 5 is based on this limiting case. In practice, the area for waste heat recovery may be smaller depending on the cost and the economic payback. Eventually, as shown in Table 5, only the cases utilizing the topping TE cycle are able to overcome the amount of power output reduction by the replacement of the cooling tower condenser with an ACC. The additional investment for waste heat recovery shows an order of magnitude larger than that of topping cycle. Fig. 9 shows the power output and the incremental investment cost as the function of the average ZT of the material. The graph shows the future potential of the TE generators when the thermoelectric properties are improved. Note that the cost axis is log scale. The ZT has a

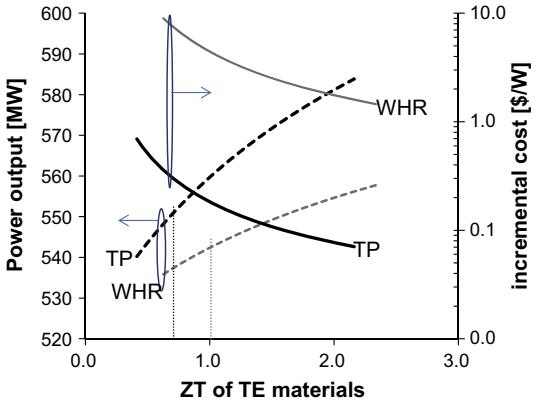

Fig. 9. Power output and incremental cost as functions of average ZT of thermoelectric material for the cases of topping cycle (TP) and waste heat recovery (WHR). ZT ~ 0.7 for TP and ZT ~ 1.0 for WHR are the typical values.

significant role in the investment cost. However, the waste heat recovery still costs much larger than the topping cycle.

7. Conclusion

This paper reports on a conceptual power-neutral method to reduce water consumption in coal-fired steam turbine power plants without sacrificing operating efficiency. The analysis model is based on a current advanced superheated steam turbine. Additional power from thermoelectric generator arrays placed on top of a Rankine cycle allows the replacement of the cooling tower condensers to the ACCs without reducing the system-level power efficiency. The ACC uses natural convection for cooling with an internal closed-loop water system and yields a 13.4 °C higher condenser temperature, hence approximately 5% of power is reduced for the Rankine cycle. The gas temperature gradient in the boiler chamber along its height is determined by a full 3-D CFD analysis to optimize the design of thermoelectric modules for maximizing the power output at each location in the boiler. The local power performance is found as a function of hot gas temperature followed by a cost analysis. The flue gas discharged waste heat recovery with thermoelectrics is also analyzed and compared to the topping cycle thermoelectrics. Due to the availability of exergy, the power output improvement with the baseline cooling tower condenser with adding the TE topping cycle and the TE FGD cycle found to be 6.0% and 4.3% (as the upper limit with fully use of available waste heat), respectively. However, the topping cycle reduces heat input to the boiler and the FGD cycle does not. This heat reduction helps to reduce the cooling load and the additional power covers the power output reduction resulting from the condenser replacement, as above, for saving the water. The available heat fluxes are different for these thermoelectric generators. Hence, the design of the thermoelectric elements is thinner for the topping cycle and thicker for the FGD cycle in order to meet the thermal resistance requirement for maximum power output.

Therefore, considering the efficiency difference, the topping thermoelectric provides a significantly (an order of magnitude) lower cost for power production compared to the waste heat recovery. The results of this analysis indicate important possible benefits to this approach, which has never been implemented in practice. In order to move toward implementation, appropriate thermoelectric materials, surface finishes, heat exchange design, good electrical contacts, and interface materials for this high temperature application will require intensive future study.

Acknowledgements

Authors MH and TSF gratefully acknowledge support from the US Department of Energy and General Motors under the Waste-Heat 2 project. Authors KY and AS gratefully acknowledge support from the Center for Energy Efficient Materials funded by the Office of Basic Energy Sciences of the US Department of Energy.

References

[1] U.S. Energy, Information Administration. Electric Power Monthly with Data for August 2013. U.S. Department of, Energy, 2013.
[2] Zahedi A. Maximizing solar PV energy penetration using energy storage technology. Renew Sustain Energy Rev 2011;15(1):866–70.
[3] King DL, Boyson WE, Kratochvil JA. Analysis of factors influencing the annual energy production of photovoltaic systems. In: Proceedings of the Twenty-Ninth IEEE Photovoltaic Specialists Conference, 2002. pp. 1356–61.
[4] Pavlović TM, Radonjić IS, Milosavljević DD, Pantić LS. A review of concentrating solar power plants in the world and their potential use in Serbia. Renew Sustain Energy Rev 2012;16(6):3891–902.
[5] Electric Power Research Institute, EPRI Technical Update. Program on Technology Innovation: new concepts of water conservation cooling and water treatment technologies. EPRI report 1025642, 2012.
[6] Yazawa K, Shakouri A. Optimization of TE topping rankine cycles for energy economy. Appl Energy 2013;109:1–9.
[7] Kenny JF, Barber NL, Hutson SS, Linsey KS, Lovelace JK, Maupin MA. Estimated Use of Waterin the United States in 2005, U.S. Geological Survey Circular 1344, U.S. Department of the Interior, 2005. p. 52.
[8] Bell LE. Cooling, heating, generating power, and recovering waste heat with thermoelectric systems. Science 2008;321(5895):1457–61.
[9] Yang J, Stabler FR. Automotive applications of thermoelectric materials. J Electron Mater 2009;38(7):1245–51.
[10] Silaen A, Wu B, Fu D, Zhou C, Yazawa K, Shakouri A. Numerical model of thermoelectric topping cycle of coal fired power plant. In: Proceedings of the ASME 2013 4th Micro/Nanoscale Heat & Mass Transfer International Conference, MNHMT2013-22248, 2013.
[11] Electric Power Research Institute, EPRI Technical Update. Power Plant Cooling System Overview for Researchers and Technology Developers. EPRI, Report number 3002001915, 2013.
[12] Bennett GL. Section 41 Space Applications, CRC Handbook of thermoelectrics, Ed. D. Rowe, CRC Press, 1995.
[13] Shakouri A. Nanoscale thermal transport and microrefrigerators on a chip. Proc IEEE 2006;94(8):1613–38.
[14] Vining CB. Chap. 28 Silicon Germanium, CRC Handbook of thermoelectrics, Ed. D. Rowe, CRC Press, 1995. p. 329–37.
[15] Mingo N, Hauser D, Kobayashi NP, Plissonnier M, Shakouri A. 'Nanoparticle-in-alloy' approach to efficient thermoelectrics: silicides in SiGe. Nano Lett 2009;9(2):711–5.
[16] Yazawa K, Shakouri A. Optimization of power and efficiency of thermoelectric devices with asymmetric thermal contacts. J Appl Phys 2012;111:024509 [6 pages].
[17] Mengali OJ, Seiler MR. Contact resistance studies on thermoelectric materials. Adv Energy Convers 1962;2:59–68.
[18] Yazawa K, Shakouri A. Cost-effective waste heat recovery using thermoelectric systems. J Mater Res 2012;27(09):1211–7.
[19] Suhir E, Shakouri A. Assembly bonded at the ends: could thinner and longer legs result in a lower thermal stress in a thermoelectric module (TEM) design. ASME Journal of Applied Mechanics, ASME JAM-11-1237 2012;79(6).
[20] Suhir E, Shakouri A. Predicted thermal stresses in an assembly with an inhomogeneous bond, and with application to a multi-leg thermoelectric module (TEM) design. ASME J Appl Mech 2013.
[21] Aquaro D, Pieve M. High temperature heat exchangers for power plants: Performance of advanced metallic recuperators. Appl Therm Eng 2007;27(2):389–400.
[22] El-Genk MS, Tournier J-M. A review of refractory metal alloys and mechanically alloyed-oxide dispersion strengthened steels for space nuclear power systems. J Nucl Mater 2005;340(1):93–112.
[23] Cockeram BV, Hollenbeck JL. The spectral emittance and long-term thermal stability of coatings for thermophotovoltaic (TPV) radiator applications. Surface Coat Technol 2002;157(2):274–81.
[24] Zorc B, Kosec LA. new approach to improving the properties of brazed joints. Weld J 2000;79(24).
[25] Saviers KR, Hodson SL, Fisher TS, Salvador JR, Kasten LS. Carbon nanotube arrays for enhanced thermal interfaces to thermoelectric modules. AIAA J Thermophys Heat Transfer 2013;27:474–81.
[26] Cola BA, Fisher TS, Xu XF. Carbon nanotube array thermal interfaces. Ch. 6 in Carbon Nanotubes: New Research, ed. A.P. Ottenhouse, Nova Science Publishers, 2009. p. 101–18.
[27] Wasniewski J, Altman D, Hodson SL, Fisher TS, Bulusu A, Graham S, et al. Characterization of metallically bonded carbon nanotube-based thermal interface materials using a high accuracy 1D steady-state technique. J Electron Pack 2012;134(020901).
[28] Cao J, Chung DDL. Carbon fiber silver–copper brazing filler composites for brazing ceramics. Weld J 1992;71(1) [21-s].
[29] McNamara AJ, Joshi Y, Zhang ZM. Characterization of nanostructured thermal interface materials–a review. Int J Therm Sci 2012;62:2–11.
[30] Cola BA et al. Photoacoustic characterization of carbon nanotube array thermal interfaces. J Appl Phys 2007;101(5). 054313–054313.
[31] Corbin SF et al. In situ measurement of the thermal contact resistance of an al lap joint during braze processing. Metall Mater Trans A 2013:1–8.
[32] Casalegno V et al. Measurement of thermal properties of a ceramic/metal joint by laser flash method. J Nucl Mater 2010;407(2):83–7.
[33] Absi J et al. Thermal response of two-layer systems: numerical simulation and experimental validation. J Eur Ceram Soc 2010;25(4):367–73.
[34] Costescu RM, Wall MA, Cahill DG. Thermal conductance of epitaxial interfaces. Phys Rev B 2003;67(5):054302.
[35] Tong T et al. Dense vertically aligned multiwalled carbon nanotube arrays as thermal interface materials. IEEE Trans Compo Pack Technol 2007;30(1):92–100.
[36] Xu J, Fisher TS. Enhancement of thermal interface materials with carbon nanotube arrays. Int J Heat Mass Transf 2006;49(9):1658–66.
[37] ASTM D5470-01: Standard test method for thermal transmission properties of thin thermally conductive solid electrical insulation materials, ASTM International, 2001. p. 1–5.
[38] Jensen C et al. Design and validation of a high-temperature comparative thermal-conductivity measurement system. Int J Thermophys 2012;33(2):311–29.
[39] Woods MC et al. Cost and performance baseline for fossil energy plants. National Energy Technology Laboratory; 2007.
[40] Yazawa K, Shakouri A. Optimizing cost-efficiency trade-offs in the design of thermoelectric power generators. Environ Sci Technol 2011;45(17):7548–53.
[41] Tayebi L, Zamanipour Z, Mozafari M, Norouzzadeh P, Krasinski JS, Ede KF, Vashaee D. Thermal and thermoelectric properties of nanostructured versus crystalline siGe. Green Technologies Conference, 2012 IEEE, 2012. p. 1–4.
[42] Fano V. Chap. 21 Lead Telluride and Its alloys. CRC Handbook of thermoelectrics, Ed. D. Rowe, CRC Press, 1995. p. 257–266.
[43] EPA Office of Water. Case Studies of Sustainable Water and Wastewater Pricing. EPA 816-R-05-007, 2005.